Available online at www.sciencedirect.com
ScienceDirect
Cement and Concrete Research 38 (2008) 511–521
Cement and Concrete Research

New waste based clinkers: Belite and lime formulations

Fabiano Raupp-Pereira [a], Richard James Ball [b,*], Joao Rocha [c], Joao A. Labrincha [a], Geoffrey C. Allen [b]

[a] Ceramics and Glass Engineering Department, CICECO, University of Aveiro, 3810-193 Aveiro, Portugal
[b] University of Bristol, Interface Analysis Centre, Oldbury House, 121 St Michael's Hill, Bristol, BS2 8BS, United Kingdom
[c] Department of Chemistry, CICECO, University of Aveiro, 3810-193 Aveiro, Portugal

Received 25 September 2006; accepted 20 November 2007

Abstract

This work describes the formulation of new belite-based (CR2) and lime-based (CR3) cementitious materials derived from industrial wastes, such as sludges (generated in the Al-anodising and surface coating industrial processes, potable water filtration/cleaning operations and in marble sawing processes) and foundry sand.

Powder mixtures were prepared and fired at different temperatures. For comparison, similar formulations were prepared with pre-treated and commercially available natural raw materials and processed in similar conditions. The thermal process was followed by differential scanning calorimetry (DSC) and high-temperature powder X-ray diffraction (HT-XRD) studies.

The CR2 clinker was found to contain belite as the main cementitious phase, the main polymorph being identified by NMR. The CR3 clinker contained common cementitious phases, such as C_3A and C_3S, but free lime and calcium aluminium oxide sulphates were also identified by high temperature XRD and NMR.

Then the corresponding cement was prepared and the evolution of the mechanical strength with time was evaluated. The lime-based cement obtained from wastes shows a stronger hardening character than the standard material, which tends to show dusting phenomena due to the presence of a reasonable amount of free lime (as the result of its expansive reaction with ambient moisture). Some fluxing impurities (e.g. alkalis) present in the waste materials improve the overall reactivity of the mixture and induces the combination of the lime in CR3. Raman, XPS and FIB techniques were used to fully characterise the aged cements.

Keywords: Industrial wastes; Belite and lime-based clinkers; Cement properties

1. Introduction

Increasing industrial activity and rising costs of natural mineral resources, have forced the transforming industry to review the logistics of raw materials supply. The continuous demand for higher productivity indices in the global competitive world has led to a fast decrease of the available natural resources and, at the same time, to the generation of a high volume of rejects or sub-standard products, most of them not directly recyclable. Mineral extraction itself is a good example of reject production [1]. Within this scenario, new approaches that consider industrial wastes as alternative raw materials becomes interesting, both technically and economically, for a wide range of applications [2], including the fabrication of concretes and mortars [3]. Traditionally, waste products are disposed of as soil conditioners or land fill. However, there might be reusing or recycling alternatives that should be investigated and eventually implemented [4–7]. Other than the usual limited incorporation in ceramic bodies with a given shape and size, expanded clays, cement and refractory mortars offer increased capabilities for high incorporation levels of rejects, as the final products are powders [8,9]. In particular, cement fabrication also involves a huge consumption of natural raw materials (e.g. limestone and clay) and recently new waste-based formulations have been tried. The so-called eco-cement

* Corresponding author.
E-mail address: richard.ball@bristol.ac.uk (R.J. Ball).

0008-8846/$ - see front matter © 2007 Elsevier Ltd. All rights reserved.
doi:10.1016/j.cemconres.2007.11.008

Table 1
Average chemical composition (XRF, wt.%) of waste and commercial raw materials (n.d. = not determined, presumed <0.5%)

Material	Al_2O_3	SiO_2	Fe_2O_3	CaO	Na_2O	K_2O	MgO	TiO_2	ZnO	SO_3	LoI
A-sludge	35.29	1.19	1.41	2.99	0.35	0.07	0.10	0.05	0.04	16.74	40.0
W-sludge	8.69	5.3	1.01	51.56	0.00	0.20	1.48	0.14	0.03	1.07	30.0
M-sludge	0.14	0.63	0.24	54.50	0.01	0.11	0.30	0.02	0.01	–	43.0
F-sand	0.20	97.5	1.12	0.22	0.02	0.26	0.03	0.20	0.02	–	0.22
Alumina	99.30	0.17	0.37	0.02	0.00	0.04	0.00	0.06	0.01	–	n.d.
Calcite	0.00	0.00	0.07	55.80	0.00	0.01	0.22	0.01	0.00	–	43.9
Sand	0.10	99.60	0.06	0.07	0.05	0.00	0.07	0.01	0.00	–	n.d.

[10] is the best example, amongst several known cases of minor incorporation of wastes, such as fly ash and slag [11,12].

In general, the clinker is the main component of cement, and is obtained by firing the appropriate mixture of raw materials at about 1500 °C. Common phases in Portland cement clinkers are: alite ($3CaO{\cdot}SiO_2$, C_3S), belite ($2CaO{\cdot}SiO_2$, C_2S), tricalcium aluminate ($3CaO{\cdot}Al_2O_3$, C_3A), and tetracalcium aluminate ferrite ($4CaO{\cdot}Al_2O_3.Fe_2O_3$, C_4AF). Belite or sulphobelite-based cements contain the phases belite (C_2S) and tetracalcium trialuminate sulphate ($C_4A_3\bar{S}$) as their main constituents [13]. They do not contain alite or tricalcium aluminate, but may contain variable amounts of calcium aluminate ferrite. They also contain calcium sulphate ($C\bar{S}$) in amounts higher than normal in Portland cement. Several compositions are referred by different authors [14–17]. One typical composition consists of: C_2S 40%; $C_4A_3\bar{S}$ 32%; C4AF 20%; $C\bar{S}$ 8%. Sulphobelite cements may perform either as non-expansive high early strength cements, or as expansive cements, depending on the proportion of the individual phases in the clinker and the amount of interground calcium sulphate [13]. Two main advantages are generally ascribed to these types of cements [17]: (i) energy savings upon firing (maximum clinkering temperature is 1350 °C; (ii) lower volume of CO_2 emissions.

Free calcium oxide in small amounts (usually below 1 wt.%) is a regular constituent of Portland clinker, but larger amounts may be present if the maximum temperature in the production of the clinker is too low, the burning time is too short, or the CaO content in the raw material exceeds the acceptable range (lime saturation factor >100) [13]. Large amounts may cause expansion, strength loss and cracking of the hardened paste, due to a delayed hydration of free calcium oxide to calcium hydroxide, which takes place topochemically and is associated with an increase in volume. Thus, excessive amounts of free calcium oxide in clinker must be avoided. However, old cements have lime and/or pozzolans as main hardening phases and their durability is easily proved in several historical monuments and common buildings. It is then obvious than the porous structure of those mechanically weak structures accommodates larger dimensional changes without serious damage [18].

This work describes attempts to define the compositions of waste-based mixtures and the corresponding processing conditions suitable to the production of belite and lime-based cements. For comparison, and to clarify the effect of minor components, present in the waste materials, on the final products properties, similar compositions were also prepared with commercial high purity grade raw materials and used as standard samples.

2. Experimental procedure

Four waste materials were selected and characterised, namely, (i) Al-rich anodising sludge (A-sludge), (ii) sludge from the filtration/clarification of potable water (W-sludge), (iii) sludge generated in marble sawing processes (M-sludge), and (iv) foundry sand (F-sand). The foundry sand was milled and sieved through 75 μm. The other materials were used in the as-received condition. For comparison, and to clarify the effect of minor components, present in the waste materials, on the final product properties, similar compositions were also prepared with commercial high purity grade raw materials and used as standard samples. These alternative high purity grade raw materials were: Alcoa CT3000 alumina, Calcitec M1 calcite and Sibelco P 500 sand. The characterisation included chemical composition, determined by X-ray fluorescence (XRF, Philips X'UNIQUE II), thermal behaviour (DTA and TGA, Setaram) and particle size distribution (Coulter) in alcohol. The full description is given elsewhere [19] but their average chemical composition is given in Table 1.

Dried (at 110 °C) components were mixed (see proportions in Table 2) in dry conditions (for 1 h, in a porcelain jar with alumina grinding balls). Each batch contains about 100 g. Fig. 1 shows the location of the formulations in the ternary diagram S–A–C. The resulting loose powders were calcined at selected temperatures (10 °C/min heating rate, 1 h soaking). The standard clinkers (hereby distinguished by a P) were prepared in a similar manner, but using the mentioned commercial reagents.

Physical parameters of milled powders (about 2 h in a rings mill + porcelain jar) such as the specific surface area (SSA, by BET) and the wt.% retained in a fixed sieve (75 μm) were determined. ^{27}Al and ^{29}Si MAS NMR spectra were recorded at frequencies of 104.26 and 79.49 MHz respectively, on a Bruker Avance 400. ^{29}Si MAS NMR spectra were acquired with 2μs (45°) radio-frequency pulses, 60 s recycle delays and a spinning rate of 5 kHz. ^{27}Al MAS NMR spectra were acquired with short (9°) and powerful radio-frequency pulses, 1 s recycle delays and

Table 2
Compositions (wt.%) of clinkers, based on wastes and on commercial pure reagents (named P)

Mixtures	A-Sludge	W-Sludge	M-Sludge	F-Sand	Alumina	Calcite	Sand
CR2	13.0	15.0	60.0	12.0	–	–	–
CR2-P	–	–	–	–	6.5	79.4	14.1
CR3	20.0	10.0	70.0	–	–	–	–
CR3-P	–	–	–	–	9.2	89.4	1.4

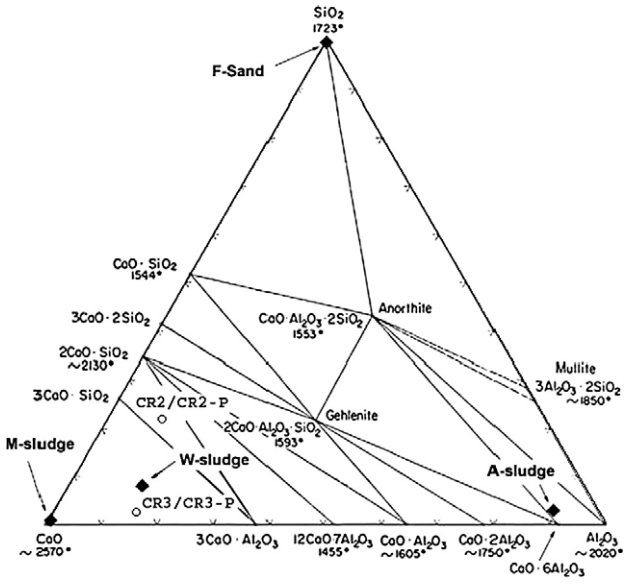

Fig. 1. Location, in the composition diagram of the SiO_2–Al_2O_3–CaO ternary system, of the wastes and the compositions investigated (CR2/CR2-P and CR3/CR3-P).

a spinning rate of 14–15 kHz. ^{29}Si chemical shifts are quoted in ppm from tetramethylsilane (TMS) and ^{27}Al chemical shifts are quoted in ppm from $Al(H_2O)_6^{3+}$.

To prepare the corresponding cement (CM) carbonate (10 wt.%) and calcium sulphate (5 wt.% hemi-hydrate) were added to the clinker before milling. Since the available amount of material is small, setting characteristics of the optimised formulations (w/c = 0.4) were inferred from temperature measurements of the fresh pastes. Samples were placed in a special thermal insulating box in order to assure almost adiabatic conditions. Temperature was continuously measured through the insertion of a thermocouple in the paste. The evolution of compressive strength with curing time was also monitored on small test bars (~20 × 10 × 8 mm) cast from the cement pastes into plastic moulds. Phases formed upon curing were determined by XRD (Rigaku Geigerflex D/max - Series, CuKα at 40 kV and 50 mA) and by DTA (Setaram LabSys). Finally, characterisation techniques were used to assess microstructural and compositional challenges of the aged cements (cured for more than 1 year). These included Raman Spectroscopy, X-ray Photoelectron Spectroscopy (XPS), and Focused Ion Beam imaging (FIB).

X-ray Photoelectron Spectroscopy (XPS) was used to characterise the outermost atomic layers on the surface of cement formulations aged for 1 and 1.5 years. Each sample was ground in an agate pestle and mortar to expose fresh surfaces for analysis. The powder obtained was compressed into holes 10 mm in diameter and 0.5 mm deep machined into a copper sample holder. The prepared samples were immediately transferred into the XPS sample introduction chamber to minimise the effects of surface contamination and reaction. An area of approximately 3 mm × 4 mm on the compressed powder surface was analysed using a Thermo VG Scientific Escascope spectrometer with an AlK_α (1486 eV) X-ray source, operated at 280 W (14 kV, 20 mA). Wide scan survey spectra were obtained between 0 and 900 eV binding energy (BE) with a step size of 1.0 eV. Subsequent high resolution scans over variable BE ranges with 0.1 eV steps were recorded for specific elements of interest: Al2*p*, Si2*p*, S2*p*, C1*s*, Ca2*p* and O1*s* regions were considered. The operating vacuum during analysis was approximately 5×10^{-9} mbar. All spectra were corrected for charging effects with respect to the adventitious hydrocarbon C1*s* peak at 284.8 eV and quantified using the sensitivity factors included with VG Eclipse operating software. PISCES version 2000.2 software was used to carry out peak fitting and quantitative analysis [20]. A linear background was assumed in all cases. The software automatically calculated the Gaussian/Lorentzian ratio to give the best fit to the photoelectron peaks.

Focused Ion Beam imaging of CM2 and CM2P cements was conducted using an FEI FIB201 focused gallium ion beam instrument, obtaining high-resolution images at 1pA beam current, 300 nm beam diameter, 10 nA, 30 keV. An organometallic gas injector was used for ion-assisted deposition of platinum over selected regions of the sample to avoid electrical charging effects produced under ion bombardment. Samples were broken by hand to produce a fracture surface prior to examination.

Raman Spectroscopy was carried out using a Renishaw Ramascope spectrometer model 2000. Analyses were carried

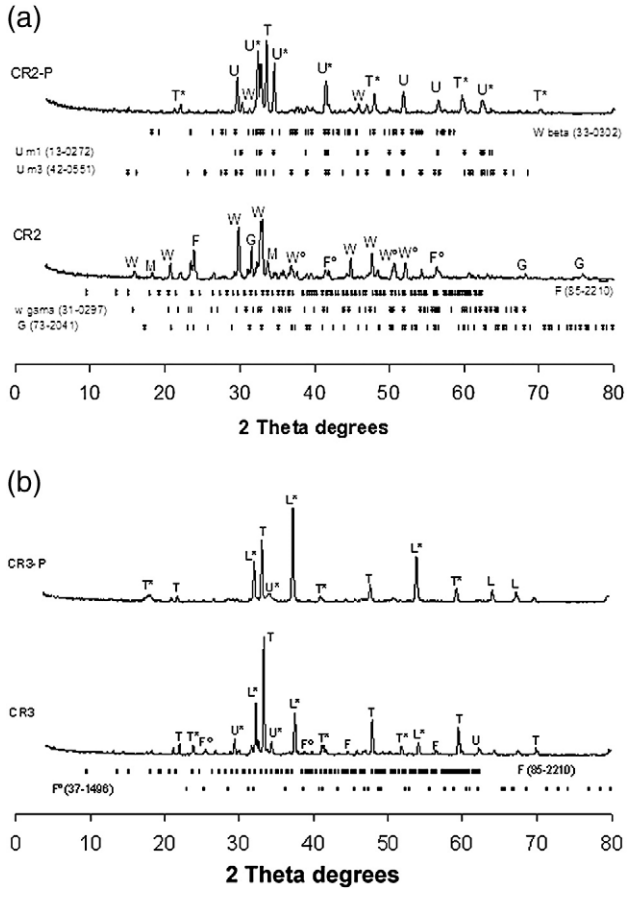

Fig. 2. (a) XRD of CR2 and CR2-P clinkers: W (γC_2S in CR2 and βC_2S in CR2-P: JCPDS 33-0302); W° (W+G); F (calcium sulphoaluminate); F° (W+F), M (mayenite, $C_{12}A_7$); U (alite; C_3S: M1 — JCPDS 13-0272 e M3 — JCPDS 42-0551), U* (U+W), T (C_3A: JCPDS 38-1429); T* (T+U). (b) XRD of CR3 and CR3-P clinkers: W (larnite, C_2S); U (C_3S); U* (U+W); L (CaO); L* (L+T); T (C_3A); T* (T+U); F (calcium sulphoaluminate: JCPDS 85-2210); F° ($CaSO_4$: JCPDS 37-1496).

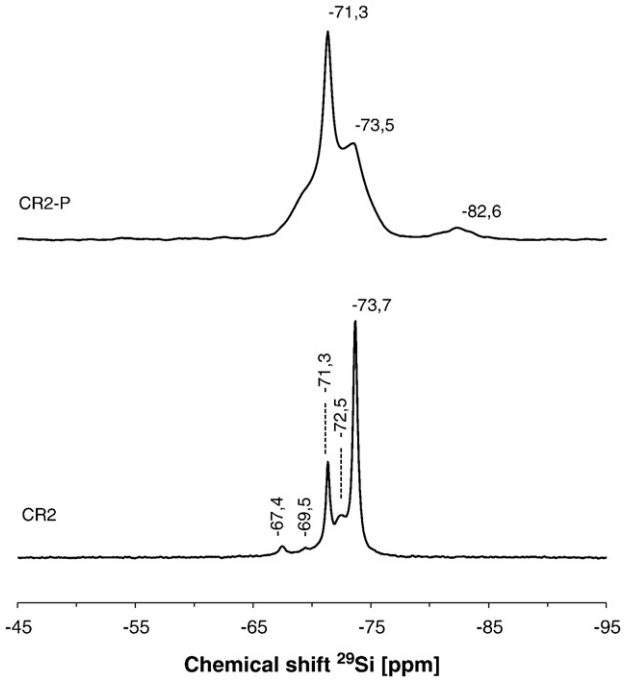

Fig. 3. ^{29}Si MAS NMR spectra of the CR2 and CR2-P clinkers.

out using a HeNe laser operating at a wavelength of 632.8 nm and maximum laser power of 25 mW, and a HeCd laser operating at 325 nm and maximum laser power of 20 mW. The analyses were performed by focussing the laser with objective magnification x 50 onto the sample surface through an Olympus BH2-UMA optical microscope, corresponding to a laser spot diameter of about 4 μm. The laser power at the specimen surface was of the order of 3 mW and an acquisition time of 10 s was used for each spectrum over the wavenumber range 200–3800 cm^{-1}. Prior to the analysis, the spectrometer was calibrated using a monocrystalline silicon standard specimen. Peak fitting and deconvolution of Raman spectra were performed using GRAMS32 software.

3. Results and discussion

3.1. Processing and characterisation of clinkers

3.1.1. Belite-based formulations

The CR2 clinker belongs to the compatibility triangle C_2S–C_3S–C_3A in the S–A–C system (see Fig. 1) and those are the solid phases to be expected, if equilibrium is established. Within this triangle, melting starts at 1470 °C (i.e. slightly above the firing temperature = 1450 °C). Equilibrium in the solid state is more difficult to achieve and neighbouring phases richer in alumina (e.g. $C_{12}A_7$ or even C_2AS) might appear as transient phases.

Fig. 2a compares the very complex powder XRD patterns of CR2 and CR2-P clinkers. Terms such as W° (W + G) mean that peak is common to both phases. CR2-P contains the expected hydraulic phases (C_2S, C_3S and C_3A), while CR2 contains, in addition to C_2S and gehlenite, $C_{12}A_7$ and calcium aluminium oxide sulphate. This mismatch is certainly due to a sluggish tendency to equilibrium in the solid state and the presence of other minor constituents in the waste materials. This waste-based CR2 clinker predictably contains a higher amount of sulphur but less than 0.2 wt.% $Na_2O + K_2O$ (just balancing the amounts contained in the starting wastes). The relatively low amount of alkalis might contribute to the low stability of the high temperature C_2S polymorphs (alpha) [21], while the high amount of sulphur (>2 wt.% as SO_3) led to the formation of calcium aluminate oxide sulphate. Those phases are well known by their expansive characteristics and might be responsible for the observed dusting tendency of CR2 samples.

NMR technique has also been used to clarify the structure of cementitious phases, mostly after hydration [22,23]. With clinkers, these studies are scarce [24]. So to begin with, common phases in Portland-type cement clinkers (C_2S, C_3S, C_3A, and C_4AF) were prepared with pure chemical reagents and characterised, to be used as references, aiming at an easier characterisation of the actual complex clinkers.

Usually, ^{29}Si and ^{27}Al chemical shifts due to structural changes induced by the incorporation (substutional or interstitial) of foreign elements in the matrix are used as references. ^{29}Si NMR spectra exhibit peaks in the chemical shift range of −69 to −75 ppm. C_2S polymorphs show single peaks at −70.3 (αC_2S), −71.4 (βC_2S) and −73.5 ppm (γC_2S) and C_3S polymorphs also show single peaks in the same region (−69.3, −72.0, −73.0, −73.7, −73.9, −74.2 and −74.8 ppm), which makes their identification difficult [24]. With the exception of $CaO.6Al_2O_3$ (CA_6), which contains octahedral Al groups (Al-VI), anhydrous calcium aluminates contain only tetrahedral Al groups (AlO_4 or Al-IV) displaying a single peak in the chemical shift range of 78 to 85 ppm. However, Al-VI groups are present in the corresponding hydrates, showing peaks at about 12 ppm [24].

Fig. 3 compares the ^{29}Si MAS NMR spectra of the CR2 and CR2-P clinkers. Two major peaks between −70 and −75 ppm can be observed. Such chemical shifts correspond to Q^0 or Q^1 mono-silicates, totally depolymerised tetrahedra. The βC_2S polymorph (peak at −71.3 ppm) and the C_3S phase (peak at −73.5 ppm) are present in both CR2 and CR2-P, but the latter seems to be a better crystallised material (sharper resonances) and contain a higher amount of C_2S (higher peak area). In the waste-based clinker, the peaks at −67.4 and −69.5 ppm are attributed to Q^0 and Q^1 sites in crystalline silicates, also presumed in the broad shoulder between −67 and −69 ppm in the C1 spectrum. In CR2, the clear presence of γC_2S (peak at −73.7 ppm) may also contribute to dusting behaviour of this powder when exposed to ambient conditions. The delay in the setting process displayed by the CR2 clinker (see Table 3) may also be explained by its lower C_2S content. The peak at about

Table 3
Initial setting time and mechanical strength development upon curing of cements

Property	CM2	CM2-P	CM3	CM3-P
Initial setting time (min)	≅660	≅312	≅521	≅540
Compressive strength after 7 days (MPa)	3.12	5.32	15.41	–
Compressive strength after 28 days (MPa)	3.22	10.49	23.33	–

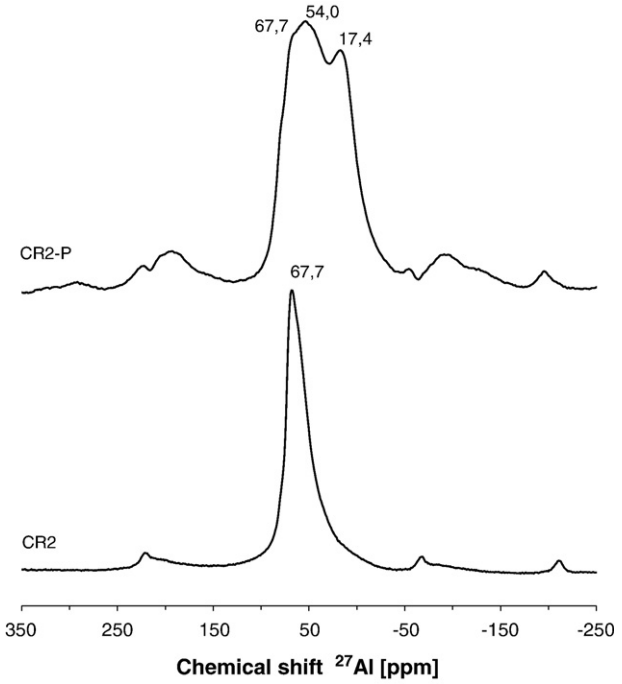

Fig. 4. ^{27}Al MAS NMR spectra of the CR2 and CR2-P clinkers.

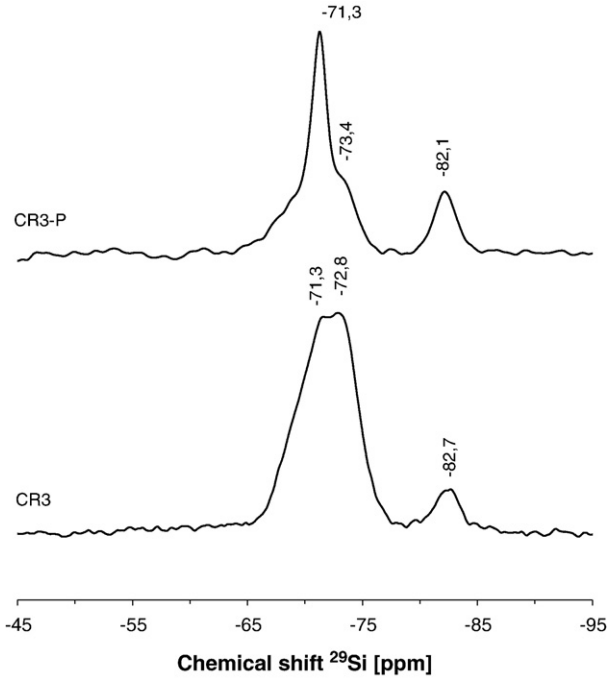

Fig. 5. ^{29}Si MAS NMR spectra of CR3 and CR3-P clinkers.

−82 ppm in the CR2-P spectrum is attributed to the presence of C–S–H hydrates [22] and confirms the higher reactivity of the standard formulation when exposed to moisture at ambient conditions. CR2 also contains gehlenite (C_2AS), identified by the peak at −72.5 ppm and also detected by powder XRD (Fig. 2a). This phase is a non-equilibrium phase and does not exhibit a hydraulic character.

The ^{27}Al MAS NMR spectrum of the CR2 clinker (Fig. 4) shows a peak at 67.7 ppm which, using the XRD information, can be attributed to $C_{12}A_7$. Besides $C_{12}A_7$, the spectrum of the CR2-P sample exhibits extra peaks, attributed to C_3A (peak at 54.0 ppm) and probable hydrates (peak at ca. 17 ppm).

Given the rather low iron oxide content of the raw materials, it is not surprising that the presence of C_4AF was not detected in CR2.

To summarise, Table 4 gives main identified phases in the clinkers by the two techniques.

3.1.2. Lime-based formulations

The CR3 clinkers lie in the primary phase field of lime (CaO), in the compatibility triangle C–C_3S–C_3A, within which melting starts at 1470 °C (i.e. above the firing temperature that was 1450 °C). However, equilibrium in the solid state is more difficult to establish with such complex waste-based materials and non-equilibrium phases are to be expected.

Once cooling is complete, $\beta C_2S + C_3A + C_3S$ are detected hydraulic phases (Fig. 2a), but calcium sulphoaluminate, calcium sulphate, and CaO are also detected by XRD, the first two just in CR3. The persistence of CaO was expected from the location of this composition in the C–A–S ternary diagram. The

Table 4
Summary of main detected phases on clinkers by using distinct techniques

Clinker	XRD	NMR
CR2	C_2S; $C_{12}A_7$; C_2AS; calcium aluminium oxide sulphate	β–C_2S; γ-C_2S; C_3S; $C_{12}A_7$; C_2AS
CR2-P	C_2S; C_3S; C_3A	β–C_2S; C_3S; C_3A; C–S–H; C–A–H
CR3	β–C_2S; C_3S; C_3A; C; calcium aluminium oxide sulphate	C_2S; C_3S; C_3A; $C_{12}A_7$; C–S–H; C–A–H
CR3-P	C_3S; C_3A; C; β–C_2S	C_2S; C_3S; C_3A; $C_{12}A_7$; C–S–H; C–A–H

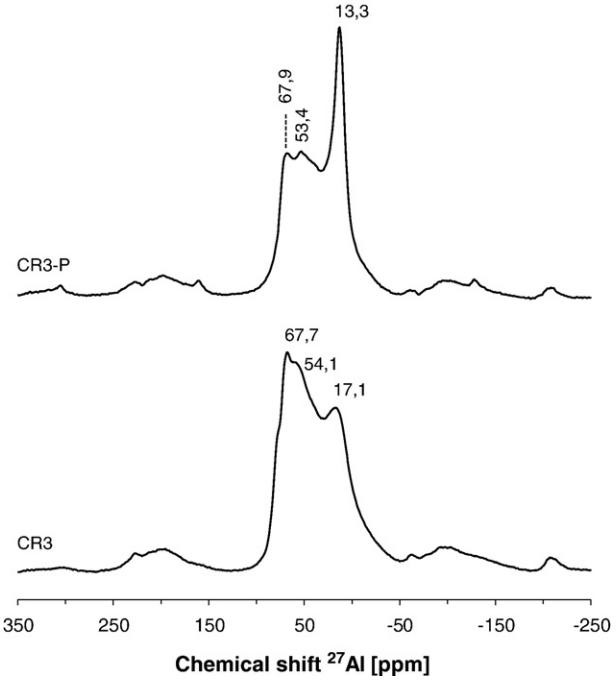

Fig. 6. ^{27}Al MAS NMR spectra of CR3 and CR3-P clinkers.

absence of γC_2S guarantees the mechanical stability of the CR3 clinker (no dusting). The presence of sulphate means that the firing schedule was not fully effective in decomposing the SO_x-containing components.

CR3-P tends to dust, due to the high relative amount of free CaO, which is known to undergo an expansive reaction with moisture. Despite the greater complexity of the waste-based clinker CR3, its expected stronger reactivity during firing (due to the presence of fluxing/mineralising components, such as alkali oxides — see Table 1) might enhance the overall stability of the material in comparison with the pure CR3-P clinker (i.e. CR3-P is likely to contain more free lime).

The ^{29}Si MAS NMR spectra of CR3 and CR3-P clinkers (Fig. 5) indicate that both samples contain the same type of phases. CR3 shows a major peak at -72.8 ppm, attributed to C_3S, and a second resonance at −71.3 ppm assigned to C_2S, in agreement with XRD evidence (Fig. 2b). These compounds are also detected in the CR3-P clinker (peaks at −71.3 and −73.4 ppm for C_2S and C_3S, respectively). The resonance at ca. −82 ppm in both spectra may be attributed to C–S–H hydrates.

Fig. 6 shows the ^{27}Al MAS NMR spectra of CR3 and CR3-P clinkers. In both cases, the major peaks appear at the same chemical shifts, despite the greater complexity of the CR3 clinker. The peaks at 67.7 ppm and 67.9 ppm are attributed to $C_{12}A_7$, despite the fact that this compound is not detected by XRD. As expected, the C_3A resonance is clearly visible at 54.1 ppm and 53.4 ppm for CR3 and CR3-P, respectively. In both cases, the formation of hydrates can be detected as peaks at ca. 17.1 and 13.3 ppm.

A summary of identified phases by different techniques is again given in Table 4.

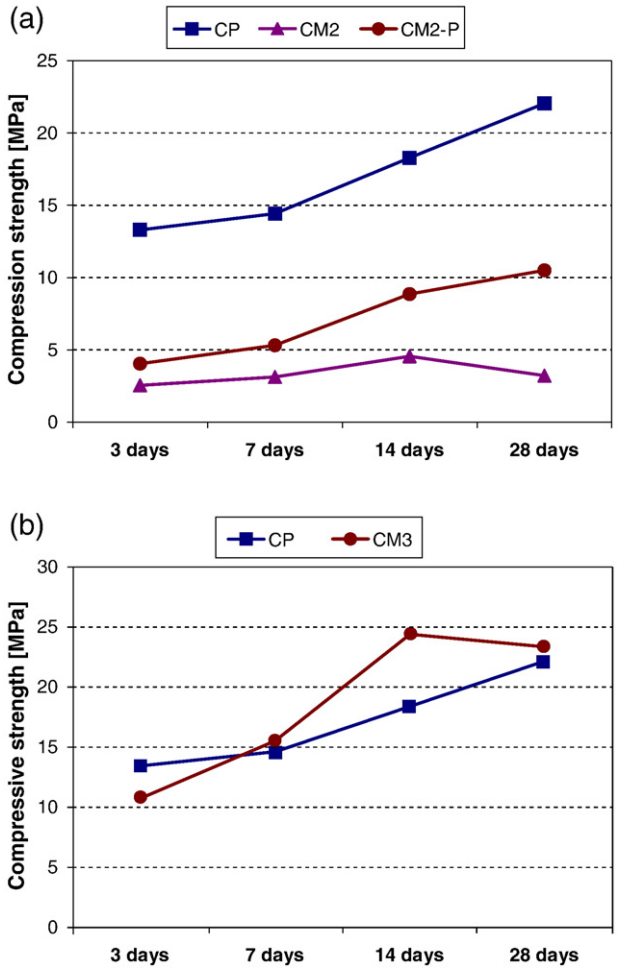

Fig. 7. Evolution of the compressive strength of cements with curing time: (a) CM2 and CM2-P formulations; (b) CM3 formulation. For comparison results obtained for Portland cement, CP, in similar curing conditions are given.

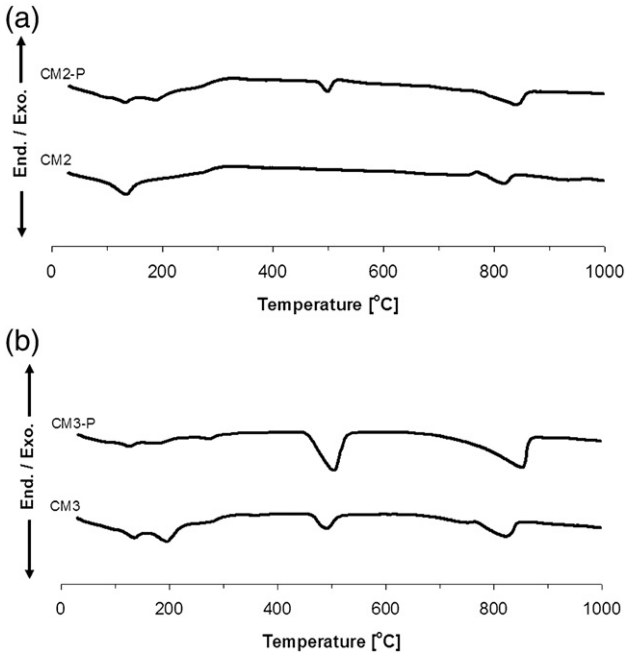

Fig. 8. DTA curves of cements after 28 days of curing: (a) CM2 and CM2-P formulations; (b) CM3 and CM3-P formulations.

3.2. Behaviour of cements

3.2.1. Belite-based formulations

Table 3 shows some characteristics of CM2 and CM2P cements. Fig. 7a shows the evolution of their compressive strength with curing time. These values are much lower than those reported for Portland cement (about 10% after 7 days of curing), meaning that the hardening process is much slower. However, long-term resistance is more comparable. For example, samples cured for 18 months show compressive strength of about 40 MPa.

Comprehensive characterisation of the 28 day aged samples was conducted by different techniques. By DTA (see Fig. 8a), decomposition reactions (between 100 and 350 °C) of C–A–H and C–S–H hydrates seem to be stronger in CM2-P, revealing their presence in higher amounts. The absence or small expression of such kind of peaks in CM2 cement is compatible with its weak hydraulic character.

Main differences between 7 and 28 day aged CM2 and CM2-P (Fig. 9a) samples measured using XRD are: (i) CM2 the main aluminate detected is mayenite ($C_{12}A_7$), less reactive than C_3A, noticed in CM2-P; (ii) CM2 contains poorly hydraulic gehlenite and calcium sulphoaluminate phases; (iii) CM2-P contains alite

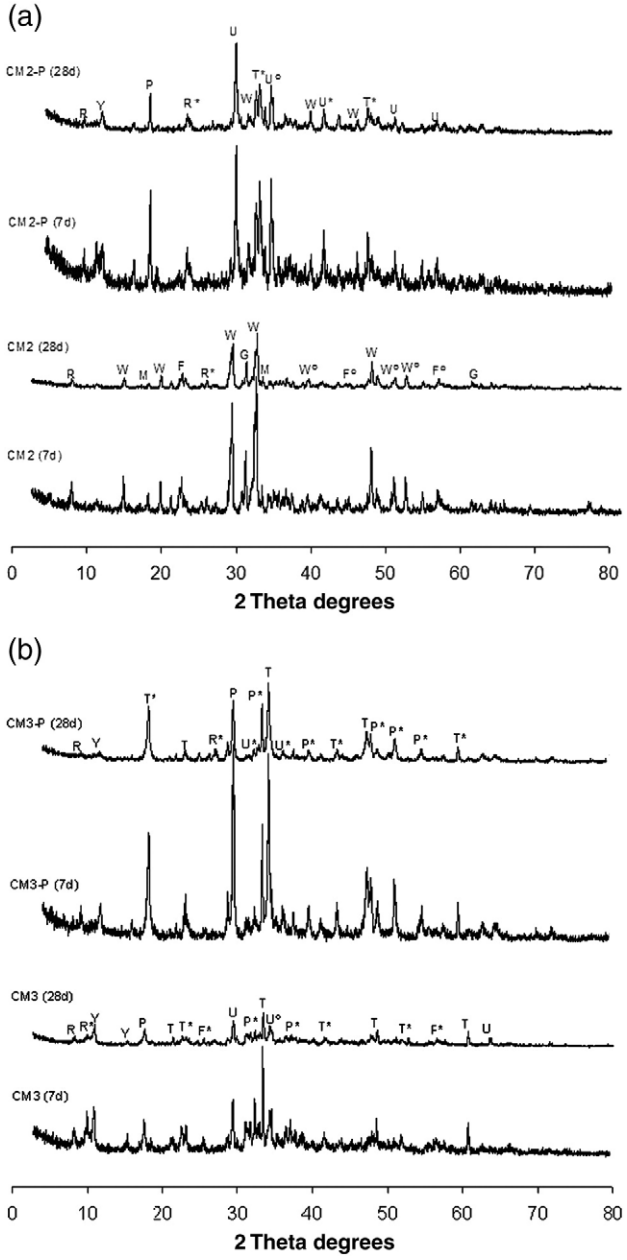

Fig. 9. (a) XRD spectra of CM2 and CM2-P cements after 7 and 28 days curing: W (larnite, C_2S); G (gehlenite, C_2AS); W° (W+G); F° (W+F); F (calcium sulphoaluminate); M (mayenite, $C_{12}A_7$); R (S–C–H); R* (R+W); U (alite, C_3S); U* (U+W); U° (U+W+P); T (tricalcium aluminate, C_3A); T* (T+U); Y (C–A–H); P (portlandite, CH). (b) XRD spectra of CM3 and CM3-P cements after 7 and 28 days curing: W (larnite, C_2S); U (C_3S); U* (U+W); U° (U+W+P), T (C_3A); T* (T+U); F (calcium sulphoaluminate); F* ($CaSO_4$); P (portlandite, CH); P* (P+T); Y (C–A–H); R (C–S–H); R* (R+W).

(C_3S) as main silicate, known for its rapid hardening character (as C_3A). As a consequence, C–S–H and C–A–H peaks are stronger in CM2 cement.

Raman spectroscopy was used to characterise CM2 and CM2-P cements after curing for more than 1 year. Fig. 10 shows spectra obtained from each cement type using a HeNe 632.8 nm laser. Both spectra are very similar and contain all the same major peaks. Raman bands associated with the ν_1, ν_2, ν_4 and ($\nu_3-\nu_1$) vibrations of the [CO_3^{2-}] molecule in calcium

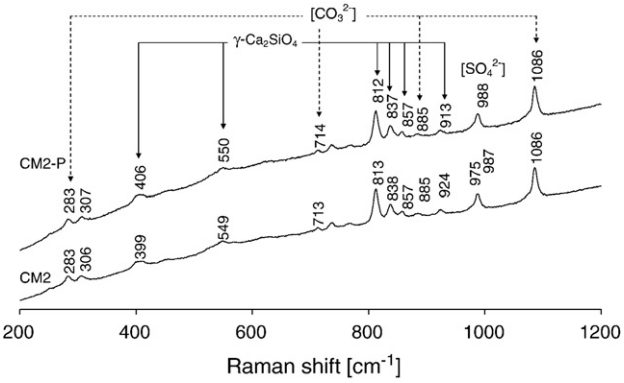

Fig. 10. Raman spectra of CM2 and CM2-P cements after over 1 year of curing obtained using a 632.8 nm red laser.

carbonate are located at 1086, 885, 714 and 283 cm^{-1} respectively. Since the curing was conducted in room conditions, carbonation might occur after long periods. In sample CM2 the ν_4 vibration was located at 713 however this small shift is within acceptable tolerances [25]. A band located at 988 cm^{-1} corresponds to the ν_1 vibration of the [SO_4^{2-}] group in ettringite [26]. Bands located at or around 181, 306, 399, 411, 550, 813, 838, 857, 885 and 924 cm^{-1} all correspond with those identified in the γ–Ca_2SiO_4 Raman spectrum [25]. The strongest peak from this phase, located at 813 cm^{-1}, which distinguishes it from the α and β forms of C2S corresponds to (A_g) symmetrical stretch. The Raman band at 738 cm^{-1} corresponds to a medium intensity band of ν_1 [(Fe, Al)O_6^{5-}], or C–S–H gel [Fe, Al)O_6^{9-}] in calcium aluminoferrite. However, the weak-medium band at 308 cm^{-1} is not clearly visible due to overlap with the 306 cm^{-1} γ–Ca_2SiO_4 band and a medium intensity band at 256 cm^{-1} [26], suggesting that these phases are present in relatively low concentrations compared to the other phases identified.

Fig. 11 shows Raman spectra for samples CM2 and CM2-P aged for over 1 year obtained using a 325 nm HeCd UV laser. A peak at 3617 cm^{-1} is visible on the spectrum corresponding to the CM2-P cement and indicates [OH^-] [27–30]. No peaks were observed at Raman shifts higher than 2000 cm^{-1} on the spectrum obtained for cement CM2. Peaks are visible around 1085 and 990 cm^{-1} for the CM2 and CM2-P cement relating to the ν_1

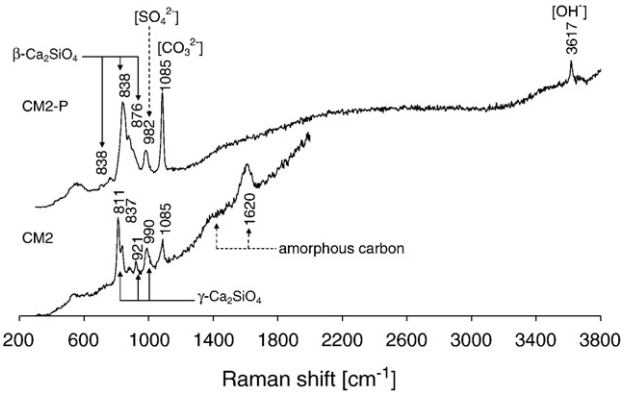

Fig. 11. Raman spectra of CM2 and CM2-P cements after over 1 year of curing obtained using a 325 nm UV laser.

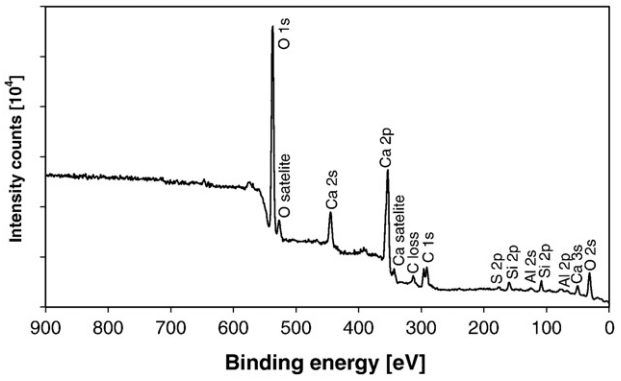

Fig. 12. XPS wide scan of 1.5 year cement CM-2P.

vibrations of the $[CO_3^{2-}]$ group in calcium carbonate and the ν_1 vibration of the $[SO_4^{2-}]$ group in ettringite [26]. Raman bands located between 800 and 900 cm^{-1} correspond to dicalcium silicate. The highest intensity peak in this region occurs at 811 cm^{-1} and 838 cm^{-1} in samples CM2 and CM2-P suggesting the presence of the γ and β forms respectively. Broad peaks located around 1620 cm^{-1} are assigned to amorphous carbon [31].

Fig. 12 shows a wide survey spectrum from sample CM2-P which is typical of all the cement sample XPS spectra. The binding energy corresponding to peaks from Al2*p*, Si2*p*, S2*p*, C1*s*, Ca2$p_{3/2}$ and O1*s* electron transitions were determined and these then used to carry out quantitative analyses. Table 5 shows calculated values for atomic % of each element and the charge corrected binding energies. Comparison of the peak positions were made with data from the Handbook of X-ray Photoelectron Spectroscopy [32].

The most abundant element identified was oxygen followed by calcium and carbon. Aluminium, silicon and sulphur were present in lower quantities, less than 6 atomic %. Marginal differences in binding energy are present between the samples analysed. Binding energies for Ca2$p_{3/2}$ peaks for all the samples lay within the range 347.0 to 347.2 eV. These values are consistent with β-dicalcium silicate. An increase in the binding energy of Ca2$p_{3/2}$ between a fresh and 2 year old sample ranging from 246.9 to 347.3 eV has been reported previously [33]. The observed increase in binding energy was attributed to hydration. The higher binding energy values in this study are consistent with a hydrated sample greater than 1 year old. The similar Ca2$p_{3/2}$ binding energies suggest that the crystal form of dicalcium silicate, either β which was observed in sample CM2-P or the γ form which was present in sample CM2, does not have a significant influence when considering the cement samples in this study.

Table 5
XPS Data of CM2 and CM2-P cements

Charge corrected binding energy	Al2*p*	Si2*p*	S2*p*	C1*s*	Ca2*p*3/2	O1*s*
CM2-1Y	74.1	100.7	169.	289.5	347.2	531.3
CM2-1.5Y	74.2	102.3	169.4	289.6	347.3	531.3
CM2-P-1Y	74.4	102.5	169.6	289.9	347.5	531.5
CM2-P-1.5Y	74.2	102.1	169.7	289.7	347.0	531.2
Normalised Atomic %	Al2*p*	Si2*p*	S2*p*	C1*s*	Ca2*p*	O1*s*
CM2-1Y	5.2	2.4	3.0	6.9	26.0	56.7
CM2-1.5Y	4.4	6.0	0.8	6.3	27.6	54.9
CM2-P-1Y	3.8	4.3	2.1	6.3	31.3	52.3
CM2-P-1.5Y	1.4	4.5	0.9	5.8	35.7	51.7

Binding energies in the ranges 289.5 to 289.9 eV and 531.2 to 531.5 eV were observed for C1s and O1s respectively. Both of these are consistent with the presence of carbonates. Binding energies ranging from 169.3 and 169.7 eV are reported for the S2*p*. This falls within the range expected for sulphates and is likely to originate from ettringite within the sample. The greatest concentration of sulphur was observed in sample CM2 suggesting the waste materials contain a greater amount of sulphur containing phases compared to the pure cement based clinkers. The atomic percentage of sulphur within the samples is significantly lower in samples aged 1.5 years compared to those aged 1 year, see Table 5.

Charge corrected peak positions for the Al2*p* peak had binding energies ranging from 74.1 and 74.4 eV, consistent with aluminium oxide. A greater proportion of aluminium was observed in sample CM2 compared to CM2-P indicating the pure phases contain a lower concentration of aluminium containing phases. It is interesting to note that a decrease in the atomic

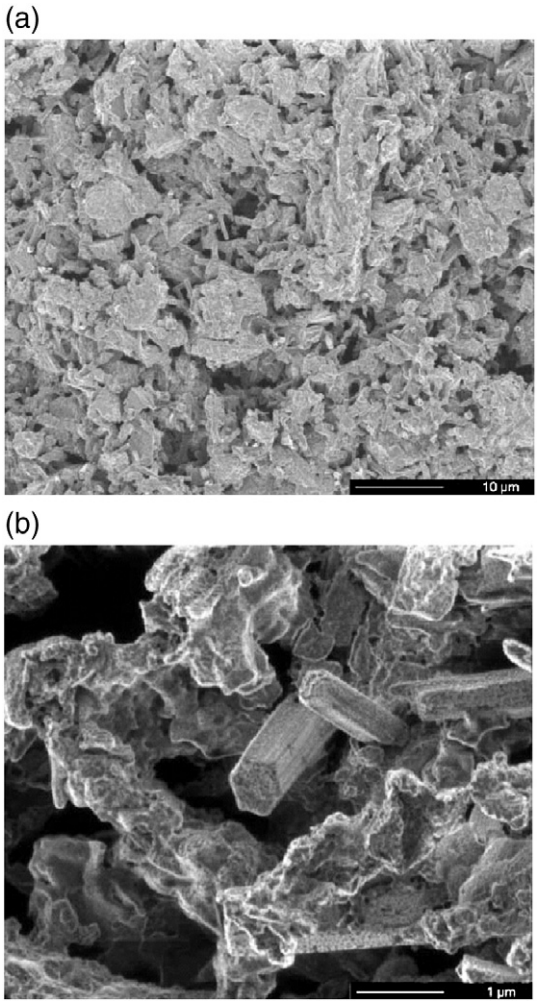

Fig. 13. Focused ion beam induced images of sample CM2: (a) 5000×; (b) 50000×.

percentage of aluminium between the 1 and 1.5 year samples is observed, similar to that observed in the sulphur.

Charge corrected peak positions for the Si2*p* peak had binding energies ranging from 100.7 and 102.5 eV.

Figs. 13 and 14 show FIB images of the internal fracture surfaces of CM2 and CM2-P cement respectively. Both mortars consist of agglomerated particles and evenly distributed pores. The agglomerates formed in cement CM2-P are noticeably larger than in cement CM2. An abundance of high aspect ratio crystals with a hexagonal cross section were observed in cement CM2 but not in CM2-P. The shape and dimensions of these crystals are consistent with ettringite [34]. At high magnification, a much denser structure is visible in cement CM2-P which is consistent with the higher strengths observed after 7 and 28 days of curing.

3.2.2. Lime-based formulations

Table 3 also shows some characteristics of these cements. Fig. 7b shows the development of the compressive strength of the cements with curing time. CM3 exhibits a good hardening behaviour, somewhat comparable to that of a commercial ordinary Portland cement. Due to dusting, CM3-P did not hardened properly and measurements were not taken. Explanations for the differences between the two formulations were firstly attempted from DTA (see Fig. 8b) and XRD (Fig. 9b) analyses, but a more comprehensive characterisation was also performed involving advanced techniques (FIB, XPS, etc).

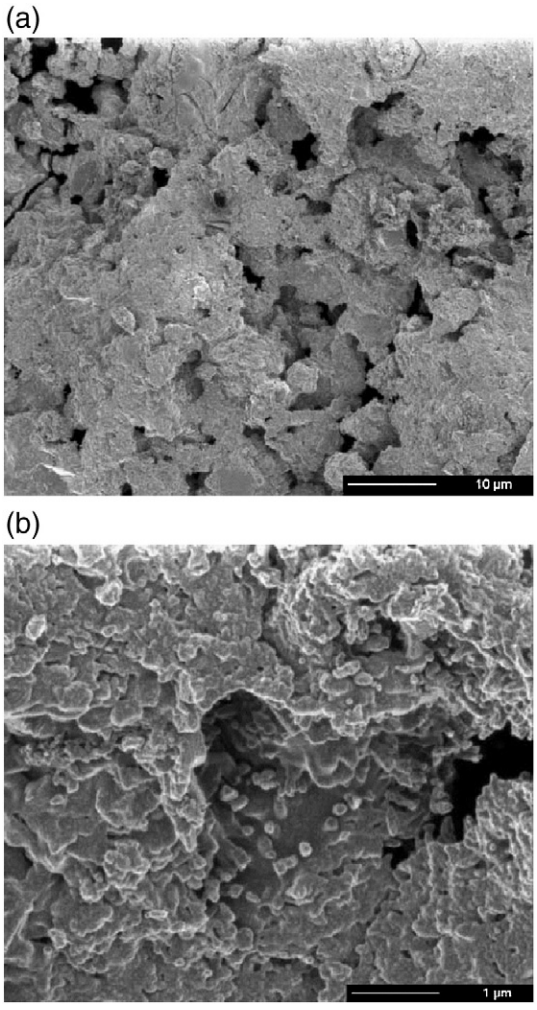

Fig. 14. Focused ion beam induced images of sample CM2-P: 5000×; (b) 50000×.

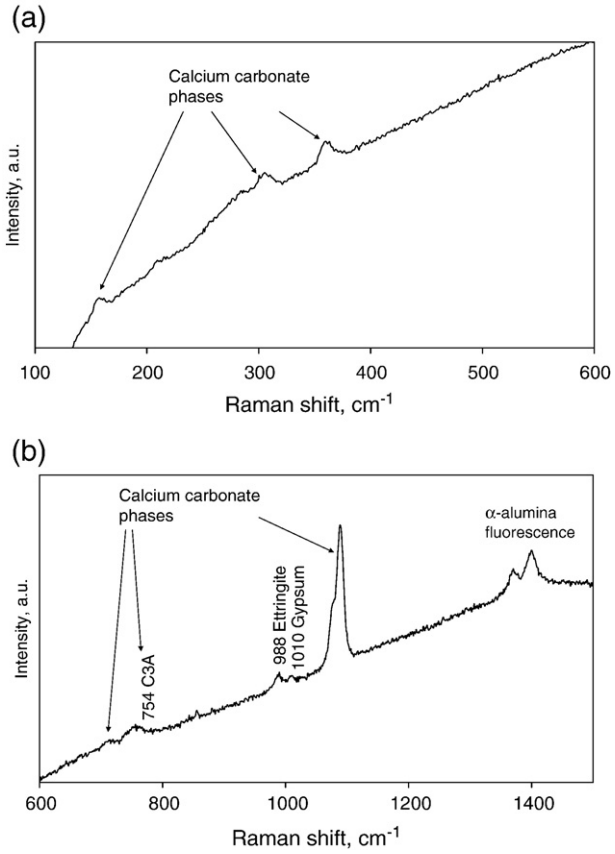

Fig. 15. Typical Raman spectrum from sample CM3-P using a 632.8 nm red laser. (a) 100–600 cm^{-1} and (b) 600–1500 cm^{-1}.

By DTA, decomposition reactions (between 100 and 350 °C) of C–A–H and C–S–H hydrates seem to be strong in both CM3 and CM3-P samples, revealing their presence in higher amounts. In CM3-P the excessive formation of CH (strong decomposition reaction at about 500 °C) is certainly responsible for the dusting phenomena since it's formation in already hardened cement paste, causes expansive reactions.

Fig. 9b compares XRD spectra of hydrated CM3 and CM3-P cements. The strong reactivity of CM3 paste is due to the increased presence of C_3A. In accordance with DTA observations, the clear detection of portlandite peaks on CM3-P seems to contribute to its weaker mechanical development, despite the presence also of other common hydrates.

Raman spectroscopy analysis using both red and UV lasers identified calcium carbonate in both the CM3 and CM3-P cements by the A_{1g} vibration of the carbonate ion at 1085 cm^{-1}. Amorphous carbon was identified in sample CM3-P by the presence of broad peaks located at 1430 and 1603 cm^{-1} in the spectra obtained using the UV laser [32]. A number of additional Raman peaks were identified in the spectra corresponding to sample CM3-P obtained using the red laser. The spectrum

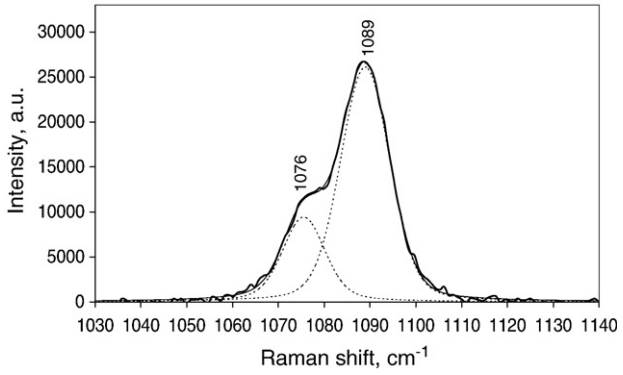

Fig. 16. Deconvolution of peaks located around 1080 cm^{-1} on Raman spectrum from sample CM3-P (see Fig. 15).

contained a high background and for this reason it is presented as two plots, 100 to 600 cm^{-1} (Fig. 15a) and 600–1500 cm^{-1} (Fig. 15b). Two peaks corresponding to the SO_4^{2-} ion located at 990 and 1010 cm^{-1} are assigned to the ν_1 vibrations of ettringite and gypsum respectively [20]. The largest peak, which contains a shoulder, has been resolved into two peaks located at 1075.7 and 1089 cm^{-1}, Fig. 16. The ratio of the intensity of these peaks is similar to that reported by Kontoyannis and Vagenas [35] for vaterite. Calcite is widely accepted as being the common form of calcium carbonate in cementitious materials and is identified by the strong ν_1 vibration at 1085 cm^{-1}. In view of its close proximity to the vaterite peaks the presence of some calcite cannot be totally discounted. Less intense peaks at 711, 280 and 157 cm^{-1}, assigned to ν_4, (ν_3–ν_1) and lattice vibrations in calcite respectively suggested the presence of calcite at low concentration [26]. Peaks at 750 and 305 cm^{-1} corresponded to vibrations assigned to vatterite [26]. This suggests that the area analysed contains calcium carbonate with structures similar to that of vaterite and calcite. This observation suggested the formation and stabilisation of vaterite in sample CM3-P but in many other areas calcite was clearly formed. Evidence of C_3A is given by the ν_3 vibration at 754 cm^{-1} [26].

XPS spectra were obtained for samples CM3 and CM3-P. The wide scan survey spectra for sample CM3-P is given in Fig. 17. Table 6 shows the charge corrected binding energies and normalised atomic percent for peaks assigned to Al2*p*, Si2*p*3/2, S2*p*, C1*s*, Ca2*p*3/2 and O1*s*. Binding energies of 74.1 and 74.5 eV were obtained for the Al2*p* peak in samples CM3 and CM3-P respectively. Both these values are consistent with aluminium oxide. Binding energies of 101.9 and 102.1 eV were obtained for the Si2*p* peak in samples CM3 and CM3-P respectively, corresponding to silicates. A binding energy of 347.1 eV for the Ca2*p*3/2 peak was obtained for both CM3 and CM3-P samples suggesting the presence of carbonates and silicates. Carbonates and aluminium oxide are suggested by binding energy values of 531.2 and 531.3 eV for the O1*s* peak for samples CM3 and CM3-P respectively. A C1*s* carbonate peak was identified at 289.5 and 289.8 eV for samples CM3 and CM3-P respectively. A binding energy of 169.4 eV observed for the S2*p* peak for both samples is consistent with sulphates. Consideration of the normalised atomic percentage values calculated indicates that the cement manufactured from the waste materials contained significantly more sulphur, silicon and aluminium compared to that from the pure materials. A higher atomic percentage of carbon was observed in the pure sample.

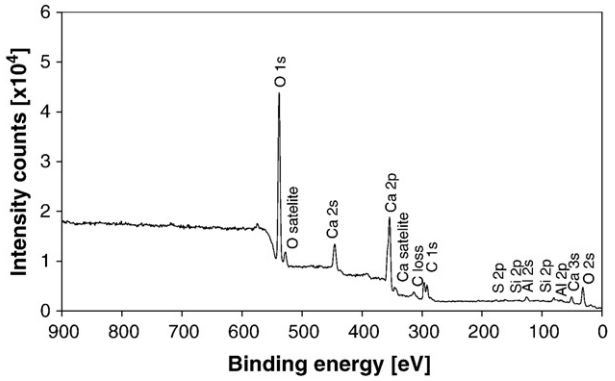

Fig. 17. XPS wide scan survey spectrum of CM3-P cement sample.

Table 6
XPS data of CM3 and CM3-P cements

Charge corrected binding energy	Al2*p*	Si2*p*	S2*p*	C1*s*	Ca2*p*3/2	O1*s*
CM3	74.1	101.9	169.4	289.5	347.1	531.2
CM3-P	74.5	102.1	169.4	289.8	347.1	531.3
Normalised Atomic %	Al	Si	S	C	Ca	O
CM3	5.4	2.6	1.9	12.1	25.9	49.9
CM3-P	3.1	1.3	0.5	17.0	31.5	44.5

4. Conclusions

The waste-based clinkers were found to contain the expected cementitious phases and a good agreement was obtained between the characterisation techniques used. In particular, the dusting phenomena observed in CR2 clinkers was explained by the formation of calcium aluminium oxide sulphate and also by the presence of γC_2S (as the result of the expansive crystallographic inversion, on cooling, of high temperature C_2S polymorphs). On its standard counter-sample (CR2-P) the βC_2S is stabilised instead. Since the total amount of alkalis in CR2-P is even lower, the non occurrence of expansive (dusting) reactions in this material means that the lack of those mineralising agents is not the controlling factor of the unwanted phenomenon. So we might conclude that sulphur content should be the determining factor, inducing the formation of detected expansive sulphur-containing phases.

Raman spectroscopy successfully identified the β and γ forms of dicalcium silicate in samples CM2-P and CM2 respectively. Evidence of ettringite in the Raman spectra is supported by observations using the FIB. XPS binding energies are consistent with the phases identified.

The lime-based cement obtained from wastes shows a stronger hardening character than the standard material, which tends to show dusting phenomena due to the presence of a reasonable amount of free lime (as the result of its expansive

reaction with ambient moisture). Some fluxing impurities (e.g. alkalis) present in the waste materials improve the overall reactivity of the mixture and induces the combination of the lime in CR3. Raman spectroscopy demonstrated the presence of both sulphate and ettringite. Calcium carbonate phases were also observed in both mixes including strong evidence for vatterite in areas of CM3-P. XPS did not identify differences in the chemical state of elements between CM3 and CM3-P samples.

Acknowledgements

Financial support by CAPES–MEC, Brazil, is greatly appreciated (F. Raupp-Pereira, Ph.D. grant). The authors also wish to thank the Council of Rectors and Coordinating Council of the Polytechnics (Portugal) and the British Council (UK) for providing funding through the Treaty of Windsor programme.

References

[1] J.M.F. Ferreira, P.M. Torres, M.S. Silva, J.A. Labrincha, in: B. Bjorkman, C. Samuelsson, J. Wikstrom (Eds.), Recycling of sludges generated from natural stones cutting processes in ceramic formulations, Proc. TMS Fall Meeting on Recycling and Waste Treatment in Mineral and Metal Processing: Technical and Economic Aspects, Lulea, vol. 2, 2002, pp. 389–395.
[2] M. Dondi, M. Marsigli, B. Fabbri, Tile & Brick Int. 13 (1997) 302–308.
[3] F. Canpolat, K. Ylmaz, M.M. Köse, M. Sümer, M.A. Yurdusev, Cem. Concr. Res. 34 (5) (2004) 731–735.
[4] D.U. Tulyaganov, S.M.H. Olhero, M.J. Ribeiro, J.M.F. Ferreira, J.A. Labrincha, Mullite-alumina refractory ceramics obtained from mixtures of natural common materials and recycled Al-rich anodizing sludge, J. Mater. Synt. Proc. 10 (2002) 311–318.
[5] D.A. Pereira, D.M. Couto, J.A. Labrincha, Incorporation of aluminum-rich residues in refractory bricks, Ceram. Forum Int. 77 (2000) 21–25.
[6] E. Martelon, J. Jarrige, M.J. Ribeiro, J.M.F. Ferreira, J.A. Labrincha, New clay-based ceramic formulations containing different solid wastes, Ind. Ceram. 20 (2) (2000) 71–76.
[7] D.M. Couto, A. Ringuedé, R.F. Silva, J.A. Labrincha, C.M.S. Rodrigues, Metallurgical sludge in clay-based fired materials, Am. Ceram. Bull. 82 (2003) 9101–9103.
[8] D.A. Pereira, J.B. Aguiar, F.P. Castro, M.F. Almeida, J.A. Labrincha, Mechanical behavior of portland cement mortars with incorporation af Al-rich salt slags, Cem. Concr. Res. 30 (7) (2000) 1131–1138.
[9] S. Pinto, K. Rosenbom, L. Machado, J.A. Labrincha, V.M. Ferreira, Incorporation of sludges in light expanded clay aggregates, Key Eng. Mater. 264-268 (2004) 1391–1394.
[10] T. Maruta, H. Ohmori, M. Moriya, K. Uchida, H. Isoda, Properties of the soil improved by the special cement made from municipal solid waste incineration ashes, Inorg. Mater. 4 (1997) 152–155.
[11] M. Kawamura, K Torii, Proc. Mater. Res. Soc. Symp. 137 (1989) 411–416.
[12] W.D. Gluchowski, W. Zajtsew, W. Pachomow, Slag-alkaline cements and concrete; structures, properties, technological and economical aspects of use, Silicate Industries 48 (1983) 197–200.
[13] I. Odler, Special Inorganic Cements, Modern Concrete Technology 8, E & FN Spon, London, 2000.
[14] K. Ikeda, Cements along the join $C_4A_3S^{-}$–C_2S, Proc. 7th ICCC, Paris, vol. 2, 1980, pp. 31–36.
[15] M.M. Ali, R. Bhargava, S.C. Ahluvalia, Hydration characteristics of magnesia assimilated sulfoaluminate-belite cement, Proc. 10th ICCC, Goteborg, paper, 2006.
[16] S. Sahu, J. Majling, Preparation of sulfoaluminate belite cement from fly ash, Cement and Concrete Research 24 (1994) 572–580.
[17] P.K. Mehta, "Investigations on energy saving cements", World Cement Technology 11 (1980) 166–177.
[18] D. Carrington, P. Swallow, Limes and lime mortars — part two, Journal of Architectural Conservation 1 (1996) 7–22.
[19] F. Raupp-Pereira, D. Hotza, A.M. Segadães, J.A. Labrincha, Ceramic formulations made of different wastes and natural sub-products, Ceramics International, 32 (2006) 173–179.
[20] PISCES Programmable Interface for Spectrometer Control Electronics, Copyright J.C.C. Day 1996-2000, Version 2000.2
[21] K. Morsli, A.G. de la Torre, M. Zahir, M.A.G. Aranda, Mineralogical phase analysis of alkali and sulfate bearing belite rich laboratory clinkers, Cem. Concr. Res. 37 (2007) 639–646.
[22] J. Schneider, M.A. Cincotto, H. Panepucci, ^{29}Si and ^{27}Al high resolution NMR characterization of calcium silicate hydrate phases in activated blast-furnace slag pastes, Cem. Concr. Res. 31 (2001) 993–1001.
[23] M.D. Andersen, H.J. Jakobsen, J. Skibsted, Characterization of white Portland cement hydration and the C–S–H structure in the presence of sodium aluminate by ^{27}Al and ^{29}Si MAS NMR spectroscopy", Cem. Concr. Res. 34 (2004) 857–868.
[24] G. Engelhardt, D. Miguel, High-Resolution Solid-State NMR of Silicates and Zeolites, John Wiley & Sons, 1987.
[25] C. Remy, B. Reynard, M. Madon, Raman spectroscopic investigations of dicalcium silicate: polymorphs and high-temperature phase transformations, J. Am. Ceram. Soc. 80 (1997) 413–423.
[26] C.S. Deng, C. Breen, J. Yarwood, S. Habesch, J. Phipps, B. Craster, G. Maitland, Aging of oilfield cement at high humidity: a combined FEG–ESEM and Raman Microscopic investigation, J. Mater. Chem. 12 (2002) 3105–3112.
[27] R.A. Buchanan, H.H. Caspers, J. Murphy, Lattice vibration spectra of Mg $(OH)_2$ and $Ca(OH)_2$, Appl. Opt. 2 (1963).
[28] M.B. Kruger, Q. Williams, R. Jeanloz, Vibrational spectra of $Mg(OH)_2$ and $Ca(OH)_2$ under pressure, J. Chem. Phys. 91 (10) (1989) 910–5915.
[29] P.H. Baranek, A. Lichanot, R. Orlando, R. Dovesi, Structural and vibrational properties of solid $Mg(OH)_2$ and $Ca(OH)_2$ — performances of various hamiltonians, Chem. Phys. Lett. 340 (2001) 362–369.
[30] T.Y. Kwon, T. Fujishima, Y. Imai, FT-Raman spectroscopy of calcium hydroxide medicament in root canals, Int. Endod. J. 37 (2004) 489–493.
[31] D.S. Knight, W.B. White, Characterisation of diamond films by Raman spectroscopy, J. Mater. Res. 4 (2) (1985) 385–393.
[32] J.F. Moulder, W.F. Stickle, P.E. Sobol, K.D. Bomben, Handbook of X-ray Photoelectron Spectroscopy, Published by Perkin-Elmer Corporation, Physical Electronics Division, 6509 Flying cloud Drive, Eden Prairie, Minnesota 55344, USA, 0-9627026-2-5, 1992.
[33] L. Black, A. Stumm, K. Garbev, P. Stemmermann, K.R. Hallam, G.C. Allen, X-ray photoelectron spectroscopy of the cement clinker phases tricalcium silicate and -dicalcium silicate, Cem. Concr. Res. 33 (2003) 1561–1565.
[34] J. Stark, K. Bollmann, Delayed ettringite formation in concrete, Bauhaus-University Weimar / Germany, available from A.G. van Os NCR, c/o WL, Delft Hydraulics, P.O. Box 177, 2600 MH Delft, The Netherlands.
[35] C.G. Kontoyannis, N.V. Vagenas, Calcium carbonate phase analysis using XRD and FT-Raman spectroscopy, Analyst 125 (2000) 251–255.